Prognostics of Rolling Element Bearings based on Cyclostationarity-based Indicators and Kalman filter under varying load and speed

Zhen Li[1,2], Panagiotis Mantas[1,2], Toby Verwimp[1,2], Alexandre Mauricio[1,2], and Konstantinos Gryllias[1,2]

[1] *KU Leuven, Department of Mechanical Engineering, Celestijnenlaan 300, 3001, Leuven, Belgium*
zhen.li@kuleuven.be
panagiotis.mantas@kuleuven.be
toby.verwimp@kuleuven.be
alex.ricardomauricio@kuleuven.be
konstantinos.gryllias@kuleuven.be

[2] *Flanders Make @ KU Leuven, Leuven, Belgium*

ABSTRACT

Rolling element bearings (REBs) are key components of rotating machines and the estimation of their remaining useful life (RUL) is crusial but still very challenging. First, fault detection should be achieved as early as possible and then the RUL should be estimated as accurately as possible. Both steps require dedicated Health Indicators (HIs), which might not be the same when looking towards detection or prognostics. A key property of REB signals is cyclostationarity, as the statistical properties of their vibration behavior vary periodically over time. This characteristic has been effectively exploited to construct HIs for anomaly detection, and fault diagnosis in the field of condition monitoring (CM) achieving high performance. Although a plethora of methodologies have been proposed for RUL estimation, they usually are restricted in cases where the load conditions are assumed steady, reducing significantly their applicability and implementation in industry. Therefore there is a clear need for methodologies that are able to estimate the RUL of REBs operating under variable or varying load and/or speed conditions. The goal of this paper is the exploration of the performance of different vibration-based HIs for fault detection, diagnosis and prognosis, including both time domain and order domain features. A dedicated bearing prognostics test rig was used to perform accelerated life tests of a self-aligned bearing, operating under varying load and speed conditions. The speed ranges from 0 to 3000 rpm and the load varies from 0 to 12 kN. The measurements lasted for around 400 hours and an outer race fault was naturally (based on overloading) generated in the loading zone of the outer race. Different signals have been acquired during the tests, including accelerations, temperature and strain signals, based on fiber optic sensors. This paper proposes a probabilistic fault detection strategy that fuses multiple HIs, rather than relying on a single one, to improve the robustness of fault onset identification. The complementarity between different HIs, such as those based on cyclic spectral coherence and cyclic spectral correlation, is explicitly exploited to enhance early detection performance and reduce false alarms. Then, this paper proposes a method to determine the optimized noise matrices for different estimators, i.e., the Extended Kalman filter (EKF), the Adaptive Kernel Kalman filter (AKKF), and the Moving Horizon Estimator (MHE). Finally, the noise matrices are used for different estimators to estimaate the RUL of the bearing.

1. INTRODUCTION

Rolling element bearings (REBs) are one of the most critical components in rotating machinery, e.g. in pumps, compressors, and wind turbines (Vencl, Gašić, & Stojanović, 2017). The prognostics of REBs helps operators schedule maintenance or replacement of these components (Wen, Fashiar Rahman, Xu, & Tseng, 2022). Consequently, the remaining useful life (RUL) estimation of REBs has attracted significant attention from academic researchers and industrial operators (Qi, Zhu, Liu, Mauricio, & Gryllias, 2024; SKF Evolution Team, 2024).

Generally, prognostics of RUL of REBs falls into three categories: (a) methods driven by artificial intelligence (Ma,

Yan, Wang, & Liao, 2023), (b) stochastic process modeling approaches (Lim & Mba, 2015; Y. Li, Huang, Ding, & Zhao, 2021; Soave, D'Elia, & Dalpiaz, 2023), and (c) physics model-based methodologies (Gabrielli, Battarra, Mucchi, & Dalpiaz, 2024). Most of these methods include 3 main steps: (1) Health indicators (HIs) extraction, (2) Fault detection, and (3) RUL estimation using different models.

Specifically, for the RUL estimation using Kalman filter (KF), a data-driven approach was proposed in (Singleton, Strangas, & Aviyente, 2015), where time and time-frequency domain features were extracted and fitted using analytical degradation models. An extended Kalman filter was then applied to predict the RUL of bearings, and validated on the PRONOS-TIA dataset under different operating conditions. Lim and Mba (Lim & Mba, 2015) proposed a Switching Kalman Filter (SKF) framework to model the degradation of bearings using multiple state-space models. Bayesian inference was employed to select the most probable degradation mode, enabling more flexible RUL prediction from in-service condition monitoring data. Cui et al. (Cui, Wang, Xu, Jiang, & Zhou, 2019) developed a Switching Unscented Kalman Filter (SUKF) to predict bearing RUL by modeling multiple operation states and dynamically selecting the most probable one via Bayesian estimation. The method improves upon traditional SKF by capturing nonlinear degradation behavior and ensuring smoother filtering outputs. Qi et al. (Qi et al., 2024) proposed a robust RUL prediction framework combining Support Vector Data Description (SVDD) for anomaly detection and Moving Horizon Estimation (MHE) for multi-step forecasting. Their method addresses issues such as HI trend instability, fault onset misidentification, and limitations of single-step estimators, demonstrating improved performance over conventional single-step estimators, including Kalman and particle filters.

Despite the notable progress made in the aforementioned literature, several critical challenges remain. First, many of the proposed approaches are developed and validated under idealized laboratory conditions with constant speed and load profiles. However, such stationary assumptions often fail to reflect the variability and complexity encountered in real-world operational environments, limiting the robustness and generalizability of these methods. Second, most existing fault detection strategies rely on a single HI as the basis for degradation tracking. While this can simplify implementation, it increases the risk of false alarms or missed detections, especially in noisy or ambiguous conditions where the chosen HI may not fully capture the evolving fault dynamics. Third, the determination of the noise covariances in Kalman-based prognostics, namely, the process noise and the measurement noise, is often heuristically tuned or left unspecified. A more systematic and adaptive strategy for identifying these matrices is essential to improve the filtering accuracy and reliability of the RUL estimation process.

To address the limitations identified above, this paper proposes a comprehensive framework for bearing degradation monitoring and RUL estimation under non-stationary operating conditions. First, a set of fault-related indicators is extracted in the order domain instead of frequency domain. This transformation effectively captures cyclostationary patterns induced by bearing faults and ensures robustness to variations in rotational speed and load. Second, a fault detection method is introduced, which leverages a probabilistic formulation across multiple HIs rather than a single metric. This multi-indicator fusion reduces the risk of false alarms and enables a more reliable detection of the fault onset. Third, the process and measurement noise in the Kalman-based estimator are determined using a data-driven multi-objective optimization procedure. Specifically, the process noise (Q) is adaptively selected to balance trajectory smoothness and consistency to observations, while the measurement noise (R) is derived from the healthy-state HI statistics. Finally, a dataset under varying load and speed is used for validation of proposed methods.

The rest of the paper is organized as follows: Section 2 presents the proposed method including HI extraction, fault detection algorithm, and the RUL estimation methodology. Moreover, in Section 3, the experimental setup and the measurements campaign are described. Furthermore the proposed methodology is applied on the experimental dataset and its results are analyzed and evaluated. The final section draws some conclusions and highlights the potential of the proposed method in the field of REBs health monitoring.

2. PROPOSED METHOD

Aiming at RUL estimation under varying speed and load, this section proposes a framework as shown in Figure 1. The first step is HI extraction, where indicators, exploiting the Enhanced Envelope Spectrum based on Correlation (EESCor), the Enhanced Envelope Spectrum based on Coherence (EESCoh), and the Improved Envelope Spectrum based on Coherence (IESCoh) (Mauricio, Smith, Randall, Antoni, & Gryllias, 2020; Mauricio & Gryllias, 2021; Antoni, Xin, & Hamzaoui, 2017), are extracted for fault detection and RUL estimation. The second step is to use all the indicators jointly to detect the fault initiation time. The third step is to use the Kalman filter to estimate the RUL based on the EESCor in which fault severity can be better represented.

2.1. HI extraction under varying speed and load conditions

When the rotational speed varies with time, the number of samples captured per revolution also changes. This non-uniform sampling introduces spectral smearing and leakage, as frequency components no longer align neatly with fixed spectral lines, making the frequency components less stable
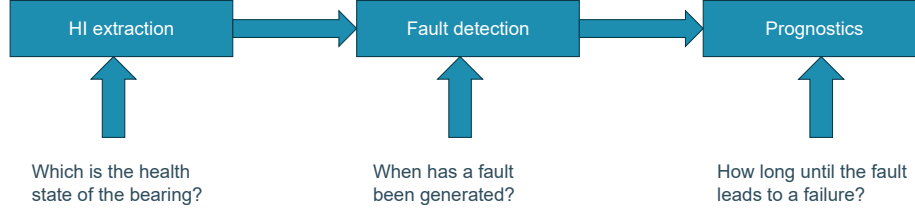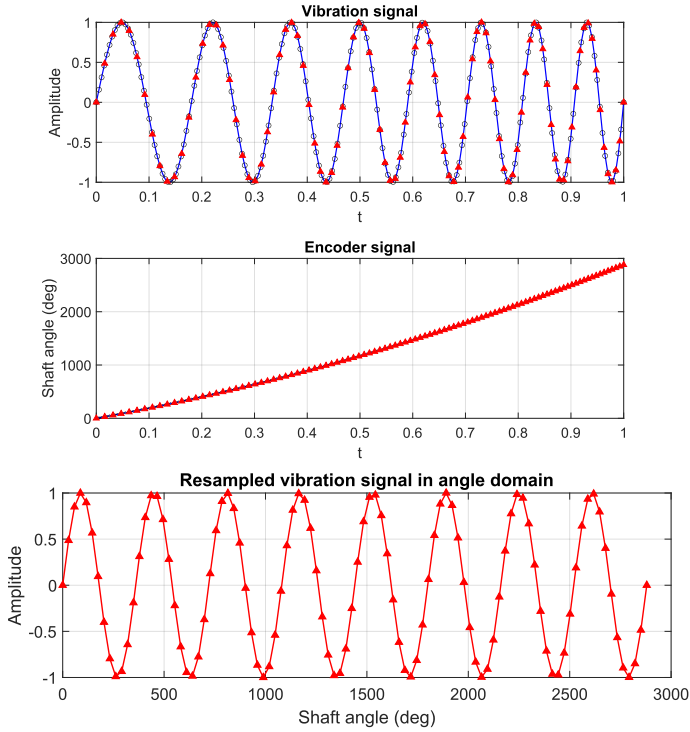
Figure 1. Framework of this paper.

Figure 2. Resampling in angle domain. (a) Raw vibration signal in the time domain; (b) Encoder signal in the time domain; (c) Resampled vibration signal in the angle domain.

or non-stationary. To address this, the signal is resampled with respect to a constant angular increment rather than uniform time steps. This ensures a consistent number of samples per revolution, independent of speed fluctuations. This transformation, which is from the time domain to the angular domain, is precisely what angular resampling achieves, as depicted in Figure 2.

Assume a signal $x(t)$ in the time domain, it can be resampled as $x(\theta(t))$ in the angle domain based on synchronized encoder signals, as shown in Figure 2. As an extended form of the definition of the CSCor (Antoni et al., 2017), the CSCor in the Order-Order domain can be calculated as:

$$CSCor_{OO}(\alpha(\theta), f(\phi)) = \lim_{W \to \infty} \frac{1}{W}\mathbb{E}\Big\{$$
$$\mathcal{F}_W\left[x(t(\theta))\right]\ \mathcal{F}_W\left[x(t(\theta + \phi))\right]^*\Big\} \quad (1)$$

where ϕ is the angle lag of θ. $\mathcal{F}_W(\cdot)$ denotes the Fourier transform in a finite time duration of W. Moreover $\mathbb{E}(\cdot)$ denotes the ensemble averaging operator. The subscript $_{OO}$ indicates that the described quantity is in the order-order domain.

To minimize the influence of energy variations and enhance interpretability, a normalization operation can be applied to the CSCor, yielding the Cyclic Spectral Coherence (CSCoh). This normalization bounds the coherence values between 0 and 1, eliminates amplitude-related distortions, and allows for consistent comparison of spectral correlation strength across different frequencies or signal conditions. The CSCoh is defined as:

$$CSCoh_{OO}(\alpha(\theta), f(\phi)) =$$
$$\frac{CSCor(\alpha(\theta), f(\phi))}{\sqrt{CSC(0, f(\phi)) \cdot CSC_x(0, f(\phi) + \alpha(\theta))}} \quad (2)$$

Both CSCor and the CSCoh can be integrated along the spectral frequency (order) axis and the corresponding envelope spectra, i.e., EESCor and EESCoh, are obtained:

$$EESCor_{OO} = \frac{1}{O_s/2} \int_0^{O_s} |CSCor(\alpha(\theta), f(\phi))|\ dO \quad (3)$$

$$EESCoh_{OO} = \frac{1}{O_s/2} \int_0^{O_s} |CSCoh(\alpha(\theta), f(\phi))|\ dO \quad (4)$$

where O_s is the angular sampling resolution after resampling. If a specific band in the CSCoh map, such as $[F_1, F_2]$ (or equivalently $[O_1, O_2]$ in the order domain), is selected for integration instead of the full range, the visibility of characteristic frequencies (orders) associated with bearing damage can be significantly improved (Wang et al., 2019; Mauricio et al., 2020; Antoni et al., 2017). Consequently, the Improved Envelope Spectrum based on coherence (IESCoh) can be obtained:

3

$$IESCoh_{OO} = \frac{1}{O_2 - O_1} \int_{O_1}^{O_2} |CSCoh(\alpha(\theta), f(\phi))| \, dO \tag{5}$$

It should be mentioned that the frequency (order) band can be selected based on different methods (Mauricio et al., 2020; Mauricio & Gryllias, 2021; Wang et al., 2019). In this paper, IESFOgram is adopted (Mauricio et al., 2020). From the resulting maps ($EESCor_{OO}$, $EESCoh_{OO}$ and $IESCoh_{OO}$), relevant indicators can be extracted by identifying prominent peaks corresponding to characteristic fault orders. These indicators provide a straightforward and interpretable representation for tracking the health state of rotating machinery.

The HIs are computed based on the sum of amplitudes of the first three harmonics of the characteristic fault frequency/order (CF or CO) extracted from $EESCor_{OO}$, $EESCoh_{OO}$, and $IESCoh_{OO}$, as defined by the following equations:

$$CO_{EESCor} = \sum_{k=1}^{3} |EESCor(k\alpha_0)| \tag{6}$$

$$CO_{EESCoh} = \sum_{k=1}^{3} |EESCoh(k\alpha_0)| \tag{7}$$

$$CO_{IESCoh} = \sum_{k=1}^{3} |IESCoh_{OO}(k\alpha_0)| \tag{8}$$

where α_0 denotes the targeted fault-related order. In this paper, α_0 corresponds to the BPOO as introduced earlier.

It is worth noting that although the external load is assumed to be able to change throughout the operation, its influence is not explicitly modeled or segmented in this paper. Therefore the HIs are carefully designed being computed as averages of the vibration energy over time windows. In specific use cases, like the one used as application in this paper, where the external load follows an apriori known periodic pattern, these short-term load fluctuations tend to cancel out during the averaging process. As a result, the derived HIs reflect the underlying degradation more clearly. This simplification enables a focused analysis of speed-dependent effects while maintaining robust degradation tracking. The influence of load variation will be addressed in future work, where more detailed modeling and segmented analysis will be explored if necessary.

2.2. Fault detection method

In this section, to determine the onset of bearing degradation, a statistical change detection method based on HIs is introduced. A period during which the bearing is confirmed to be healthy is first selected, and the corresponding HI values (e.g., EESCor, EESCoh, and IESCoh) are extracted. The best-fitting distribution for these data is identified using the Bayesian Information Criterion (BIC) from a predefined library that includes Normal, Lognormal, Exponential, Weibull, and Rayleigh distributions. This reference distribution, denoted as Dis, is used to establish a statistical baseline, and a counter is initialized. During monitoring, if five consecutive HI values exceed the upper bound (which is determined by the fitted parameters of the selected distribution) of Dis, the point is identified as the degradation onset.

2.3. RUL estimation using Kalman filter

After the fault is identified to appear, the HI, which should have the highest trendability among all HIs, is used as the observation of the Kalman filter. The flowchart of the RUL estimation using Kalman filter is shown in Figure 3. Degradation functions are combined with observations of the selected HI and processed by state estimators such as the EKF, AKKF, or MHE. These estimators identify the underlying model parameters, which are then used together with a predefined failure threshold to generate RUL particles for probabilistic RUL estimation. The algorithms of different estimators can be found in these references (Singleton et al., (2015); Qi et al., (2024); Li et al., (2025)).

It should be noted that the determination of noise covariance matrices, namely, the process noise (Q_p) and the measurement noise (R_m)—has long been a recognized challenge in the Kalman filtering community. As discussed in the literature (Zhang et al., 2020), these matrices significantly influence filter behavior by governing the balance between trusting the degradation model and relying on observed HIs.

In this study, a systematic approach is proposed to address this issue. The measurement noise R_m is assumed to reflect the variability of the system in its healthy state and is therefore estimated from the variance of the HI during the healthy period, $\mathcal{H}$, as determined in the previous section. The process noise Q_p, on the other hand, is optimized using a short segment of data from the early stage of degradation. This approach ensures that the noise matrices capture realistic model uncertainty while avoiding overfitting.

To enhance the robustness and generalization of the Kalman-based estimators, the process noise covariance Q_p is optimized through a single-objective search that balances estimation smoothness and statistical consistency with the observations. The measurement noise R_m is assumed to be known
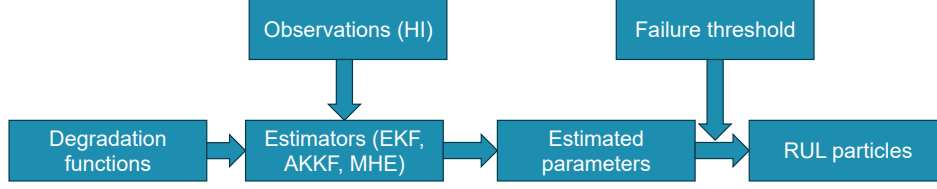
Figure 3. Flowchart of the RUL estimation.

and fixed based on the healthy-state statistics, as described earlier. The detailed steps are outlined below:

Step 1: **Definition of the candidate grid for Q_p**

To perform a grid search over candidate values of the process noise, a set of positive scalar values is defined:

$$\mathcal{Q} = \{q_1, q_2, \ldots, q_{n_q}\}, \quad q_i \in \mathbb{R}_+.$$

Each q_i represents a scalar variance parameter, which is used to construct the process noise covariance matrix. Specifically, for each $q_i \in \mathcal{Q}$, the corresponding process noise covariance matrix is defined as:

$$Q_p^{(i)} = q_i I_2 = \begin{bmatrix} q_i & 0 \\ 0 & q_i \end{bmatrix},$$

where I_2 denotes the 2×2 identity matrix. This formulation assumes isotropic process noise, i.e., equal variance in both dimensions of the process state.

The measurement noise covariance R_m is kept fixed and is estimated from the variance of the health indicator (HI) signal during a known healthy operating period:

$$R_m = \text{Var}(y_t), \quad t \in \mathcal{H} \qquad (9)$$

Here, y_t is the observed HI at time t, and $\mathcal{H}$ denotes the time interval during which the system is confirmed to be healthy.

Step 2: **Application of the estimator**

For each candidate q_i, the chosen filtering algorithm (e.g., EKF, AKKF, or MHE) is applied to the HI sequence $\{y_t\}_{t=1}^T$, yielding filtered outputs $\hat{y}_t(q_i)$. These outputs represent the estimated latent degradation trajectory. The time horizon T refers to a predefined early degradation period, which allows for reliable assessment before severe nonlinearity or noise dominates.

Step 3: **Computation of the smoothness loss**

To ensure temporal consistency and suppress estimation jitter, the second-order difference energy is

used to quantify smoothness:

$$J_{\text{smooth}}(q_i) = \frac{1}{T-2} \sum_{t=3}^{T} (\hat{y}_t - 2\hat{y}_{t-1} + \hat{y}_{t-2})^2$$

$$(10)$$

This metric penalizes abrupt local curvature, favoring stable and physically plausible degradation patterns over time.

Step 4: **Computation of the fit-to-observation loss**

The discrepancy between the estimated and the observed HI is quantified using the Mean Squared Error (MSE):

$$J_{\text{fit}}(q_i) = \frac{1}{T} \sum_{t=1}^{T} (y_t - \hat{y}_t)^2 \qquad (11)$$

While the goal is not to strictly fit the observations, this term helps ensuring that the residuals remain within a reasonable range, consistent with the Gaussian noise assumption in Kalman filtering. It reflects how well the model explains the observations under the assumed measurement noise.

Step 5: **Normalization of the objectives**

To ensure a fair combination of the two loss terms (which may differ in scale), both are normalized using min-max normalization:

$$\tilde{J}_{\text{smooth}}(q) = \frac{J_{\text{smooth}}(q) - \min J_{\text{smooth}}}{\max J_{\text{smooth}} - \min J_{\text{smooth}}} \qquad (12)$$

$$\tilde{J}_{\text{fit}}(q_i) = \frac{J_{\text{fit}}(q_i) - \min J_{\text{fit}}}{\max J_{\text{fit}} - \min J_{\text{fit}}} \qquad (13)$$

Step 6: **Computation of the total weighted loss**

The total cost is formulated as a weighted sum of smoothness and fit losses:

$$J_{\text{total}}(q_i) = \lambda_1 \cdot \tilde{J}_{\text{smooth}}(q_i) + \lambda_2 \cdot \tilde{J}_{\text{fit}}(q_i) \quad (14)$$

where λ_1 and $\lambda_2 = 1 - \lambda_1$ are user-defined trade-off parameters. This formulation allows flexible balancing between robustness (smoothness) and statistical consistency with the observed data, as expected under the Gaussian noise assumption.

Step 7: Selection of the optimal Q_p

The optimal process noise level q^* is selected by minimizing the total loss over the search grid:

$$q^* = \arg\min_{q \in \mathcal{Q}} J_{\text{total}}(q_i),$$

where $J_{\text{total}}(q)$ denotes the objective function (e.g., prediction error, likelihood, etc.) evaluated under process noise level q.

The corresponding optimal process noise covariance matrix is then:

$$Q_p^* = q^* I_2 = \begin{bmatrix} q^* & 0 \\ 0 & q^* \end{bmatrix}.$$

This value is used in the subsequent Kalman-based estimation and prediction.

3. DESCRIPTION OF THE EXPERIMENTAL SET UP AND OF THE MEASUREMENT CAMPAIGN

This section describes the measurement campaign, including an accelerated life test, carried out under varying speed and load conditions. The measurement campaign was conducted on the KU Leuven Bearing Prognostics Setup (KULBPS). As shown in Figure 4, one test bearing and two support bearings were mounted on a shaft. The test bearing was subjected to a radial force applied via an electrohydraulic actuator. Multiple types of signals were collected during the test, including vibration signals from accelerometers, strain signals from optical fibers, speed signals from an encoder, and force signals from a force cell. In this study, the acceleration signals measured by the accelerometer mounted on the test bearing housing along the radial (force) direction were specifically used for analysis. The test bearing is an SKF 2208 E-2RS1KTN9, which contains two rows of balls. Its ball pass order of the outer race (BPOO) is around 7.7.

The measurements were conducted under varying speed and load conditions. The corresponding speed and load profiles are illustrated in Figure 5. This load profile encompasses a wide range of speed and load combinations, enabling a comprehensive assessment of system dynamics and fatigue behavior, making it especially appropriate for bearing fatigue studies. The load profile was converted into analog voltage signals and transmitted to the motor and the electrohydraulic actuator drives via an MCC USB DAQ device. Data acquisition was performed using a Siemens Simcenter SCADAS Mobile system, with signals recorded for 1 minute every 6 minutes. A sampling rate of 51.2 kHz was selected to balance storage requirements and computational efficiency. The at the end failed bearing is shown in Figure 6. The expected L10 life of the bearing under this profile is around 70 hours. The bearing's lifetime was approximately 400 hours, corresponding to 4023 acquisitions (i.e., 4023×6 minutes).

Besides, in this study, the sum of the first 3 harmonics of the

Ball Pass Order of the Outer race (BPOO) are selected for constructing the HIs as shown in Equations 3–5. This choice is motivated by the fact that the test bearing used in this paper is a self-aligning ball bearing, in which outer race faults are more likely to occur under fatigue loading. This is because the outer race in such bearings lacks a guiding groove and has significantly less contact area compared to the inner race, leading to higher localized contact stresses and an increased likelihood of fatigue-induced damage.

4. EXPERIMENTAL RESULTS

In this section, the proposed method is applied, tested, validated and evaluated using the experimental bearing degradation dataset mentioned above.

4.1. HI extraction and comparison

Firstly, the vibration signal of each acquisition is converted into the angle domain as described in Section 2.1. The signals from acquisition No. 4000 are shown in Figure 7. Clear modulation behavior can be observed in Figure 7 (d), where the BPOO and its harmonics (e.g., $2 \times BPOO$, $3 \times BPOO$) are indicated by red dashed lines.

Additionally, two order regions, marked by blue dashed lines in Figure 7 (d), can be observed where the BPOO modulates resonance-related components in the order domain. These sidebands indicate that high-order components are modulated by fault-related orders such as the BPOO. This phenomenon can also be observed in the frequency domain.

For the order band selection of $IESCoh_{OO}$, the IESFOgram, a bearing diagnostics tool, is used. Figure 8 illustrates the optimal bands identified by the IESFOgram (Mauricio et al., 2020; Mauricio & Gryllias, 2021) over the last 400 acquisitions. It can be observed that after acquisition No. 3830, the selected optimal band changes. Moreover, most of the optimal bands are concentrated in the range of [42, 64] order during the final period. Consequently, this band is fixed for the computation of $IESCoh_{OO}$ in all acquisitions to enable consistent tracking of the health state changes.

In this section, several HIs are presented and their performance is discussed. As shown in Figure 9, different HIs are calculated based on the sum of the amplitude of the first three harmonics from different spectral representations including FFT, SES, EESCoh, EESCor, and IESFOgram-based IESCoh, and are presented covering the full degradation process at the left column, while a zoomed-in view of the final stage is presented on the right column.

Among them, the HI derived from the EESCor (Figure 9 (g) and (h)) exhibits the most favorable monotonic trend, with a stable baseline and a sharp, consistent rise near failure. The IESFOgram-based IESCoh (Figure 9 (i) and (j)) further improves early sensitivity. In contrast, the HIs based on tra-
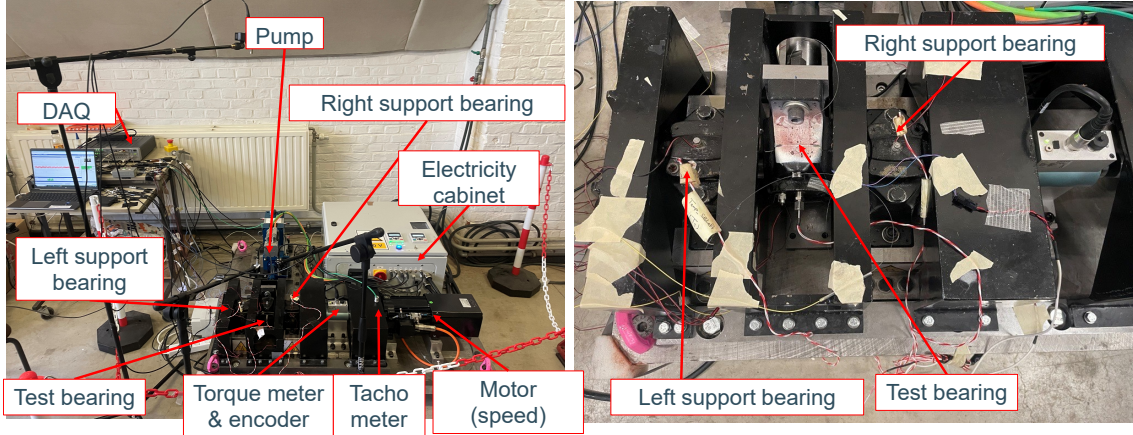
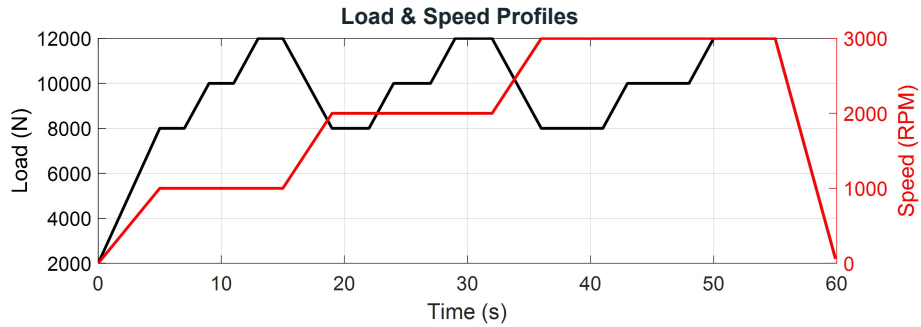Figure 4. KU Leuven Bearing Prognostics Setup.

Figure 5. Operating conditions during the measurements.

Figure 6. The defect on the outer race of the bearing at the end of the test.

ditional FFT and SES (Figure 9 (a)-(d)) display more fluctuations and less clear trends, particularly during the early and middle stages of degradation. Meanwhile, the EESCoh-based HI (Figure 9 (e) and (f)) shows good response in the early stage but tends to be unchanged before reaching the failure point. This makes it less suitable for tracking fault severity near the end of life. Overall, the proposed EESCor and IESFOgram-based IESCoh offer superior performance in

terms of monotonicity and sensitivity, which are critical for both fault detection and RUL prediction.

In the following subsections, $BPOO_{EESCor}$, $BPOO_{EESCoh}$, and $BPOO_{IESCoh}$ will be jointly used for fault detection. After the fault onset time is determined, $BPOO_{EESCor}$ will be used for RUL estimation.

4.2. Fault detection using different HIs

As illustrated in Section 2.2, the healthy stage of the bearing is defined as the initial 1000 acquisitions. The distributions of the selected HIs during this period, along with their best-fit models, are shown in Figure 10. Additionally, the fault onset times identified by the three indicators are summarized in Table 1.

Several observations can be drawn from Figure 10:

(1) Both $BPOO_{EESCor}$ (Figure 10 (d)) and $BPOO_{EESCoh}$ (Figure 10 (f)) exhibit similar fluctuations during the healthy stage, which makes the distinction between healthy and faulty conditions less clear. These indicators integrate spectral components over a wide frequency range and may be influenced by unrelated frequency content. In contrast, $BPOO_{IESCoh}$ (Figure 10 (b)) shows a more stable and distinguishable trend,
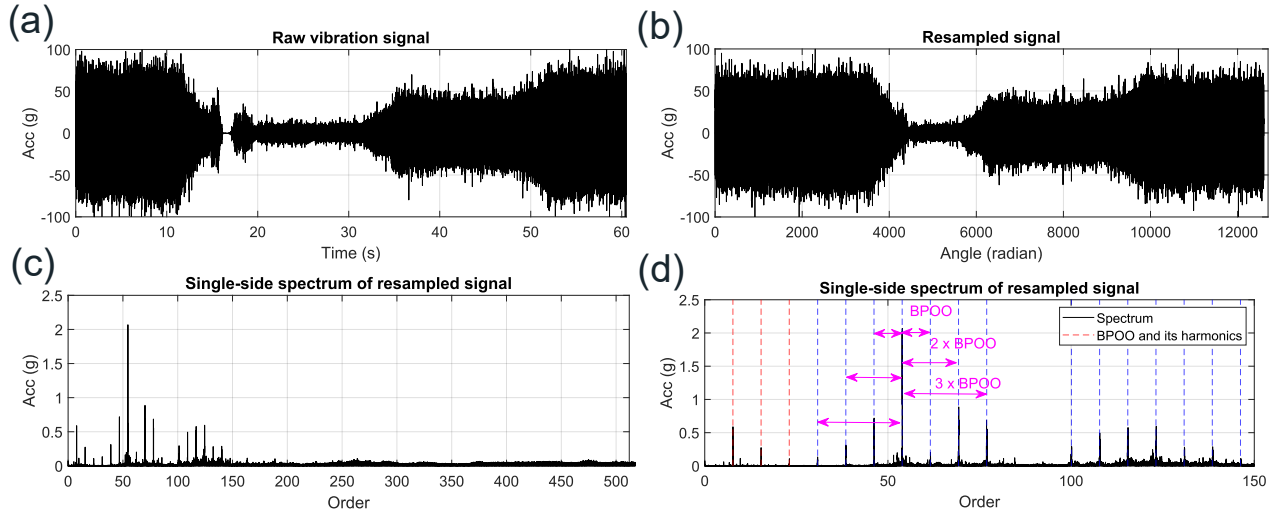
Figure 7. Acquisition No. 4000: (a) Raw vibration signal; (b) Resampled signal based on the encoder signal; (c) The spectrum of the resampled signal in the order domain; (d) The enlarged figure of (c) up to order 150.
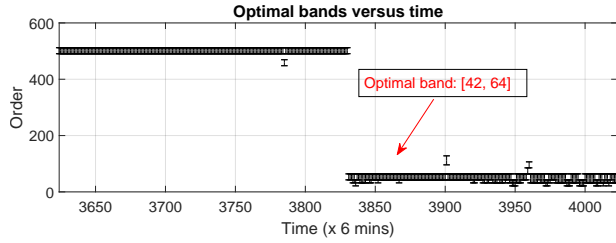

Figure 8. Optimal band selected by the IESFOgram in the last 200 acquisitions.
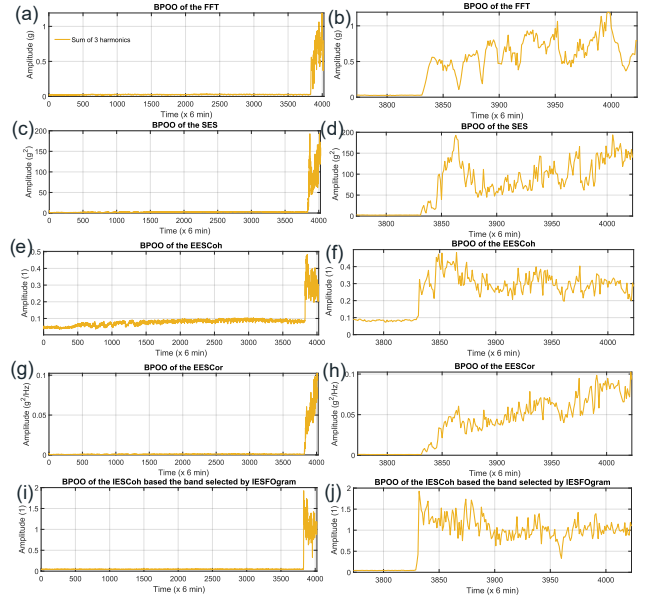

Figure 9. HIs calculated on (a) the raw spectrum and (b) zoom; (c) SES and (d) zoom; (e) the EESCoh and (f) zoom; (g) the EESCor and (h) zoom; (i) the IESCoh based on the band selected by the IESFOgram and (j) zoom.

as it specifically focuses on the band containing fault-related modulation, thereby improving fault stage identification.

(2) As shown in Figure 10, numerous isolated points (marked as red dots) exceed the anomaly thresholds across all HIs. This suggests that using isolated points for fault determination may lead to false alarms. Hence, a consecutive detection strategy, requiring multiple consecutive threshold exceedances, provides more robustness and reduces false alarms.

(3) Relying on a single HI to determine the fault onset time may be unreliable, especially when the initial degradation trend is weak or ambiguous. Therefore, a conservative fault onset at acquisition 3832 is selected based on the combined behavior of all three HIs, serving as a robust baseline for RUL estimation.

(4) Among the three indicators, $BPOO_{EESCor}$ demonstrates the most distinct and consistent degradation trend after fault initiation. Therefore, it is chosen for subsequent prognostic modeling and RUL prediction.

4.3. RUL estimation using different estimators

In this section, a single exponential model is used for RUL estimation combined with different estimators. It is cast into a discrete-time state-space form so that it can be processed by various filters (EKF, AKKF, and MHE). Table 2 illustrates the formulation: the state vector comprises the current degradation level and the rate parameter, which evolve according to a nonlinear transition function with additive process noise u_n, while the measurement equation includes observation noise v_n. The noise terms are assumed to follow Gaussian distri-
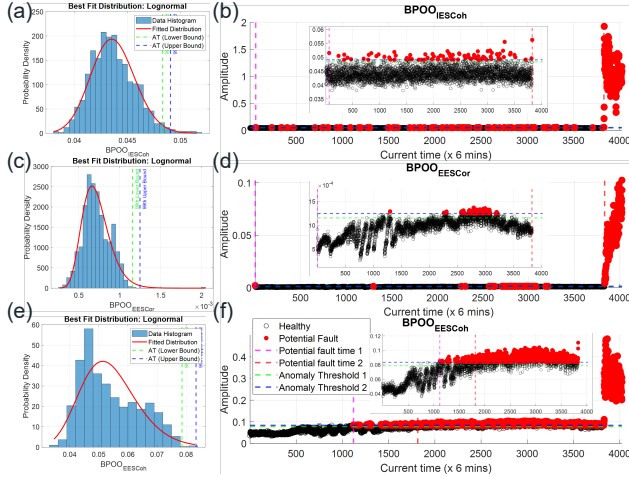
Figure 10. Fault detection using different HIs: (a) The histogram of the $BPOO_{IESCoh}$; (b) The $BPOO_{IESCoh}$; (c) The histogram of the $BPOO_{EESCor}$; (d) The $BPOO_{EESCor}$; (e) The histogram of the $BPOO_{EESCoh}$; (f) The $BPOO_{EESCoh}$.

Table 1. Fault onset time determined by HIs.

Indicators	Best distribution (BIC)	Fault onset time
$BPOO_{EESCor}$	Lognormal	3832
$BPOO_{EESCoh}$	Lognormal	1815
$BPOO_{IESCoh}$	Lognormal	3829

butions, where $u_n \sim \mathcal{N}(0, Q_p)$ and $v_n \sim \mathcal{N}(0, R_m)$, with Q_p and R_m determined using the methodology described in Section 2.3.

4.3.1. Determination of the noise matrices

In this section, the noise matrices determination method proposed in Section 2 is applied. The hyper-parameters are selected as follows: (1) To allow for longer analysis, the failure threshold is set to 0.1, corresponding to the 4022nd acquisition. In addition, $BPOO_{EESCor}$ is normalized using 0.1 to avoid numerical issues in the Kalman filter. (2) R_m is determined as the variance of the HI during the healthy period. (3) A set of 30 acquisitions after fault onset is selected as the training set for Q_p optimization. (4) The search grid for Q_p is defined as 100 logarithmically spaced values from 10^{-10} to 10^{-4}. (5) The weights $\lambda_1 = 0.7$ and $\lambda_2 = 0.3$ are used to balance smoothness and consistency. This choice reflects the need for robust trend tracking under non-stationary and noisy conditions, where overfitting to short-term fluctuations may compromise RUL stability and reliability. Finally, all estimators, i.e., EKF, AKKF and MHE, are employed in the optimization procedure.

The measurement noise, R_n, is calculated as 3.9713×10^{-6}. Figure 11 illustrates the total weighted loss $J_{\text{total}}(Q)$ with respect to the logarithm of the process noise level for the

Table 2. The degradation function used in this paper.

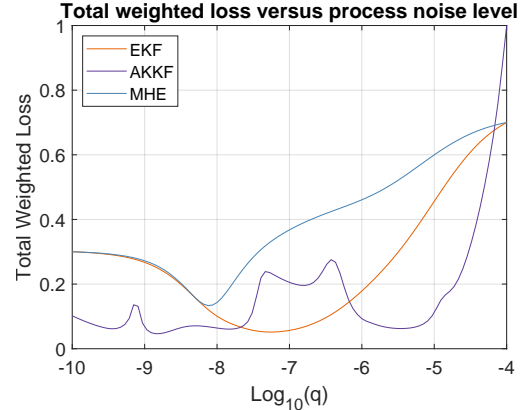| Functions	Arrangement
Single exponential (EXP1), $y = ae^{bt}$	$x_n = \begin{bmatrix} x_{n-1,1}\, e^{x_{n-1,2}} \\ x_{n-1,2} \end{bmatrix} + u_n,$ $y_n = x_{n,1} + v_n.$

Figure 11. Optimal process noise

three estimators. All three estimators exhibit a consistent U-shaped trend in the total weighted loss as the process noise level q varies on a logarithmic scale. When q is too small, the estimators tend to over-rely on the model prediction, resulting in overly smooth trajectories that deviate from the observed data. Conversely, a large q value causes the estimators to rely excessively on the noisy observations, thereby reducing the smoothness of the estimated degradation curve. Between these two extremes, each method achieves a minimum loss at a specific q, indicating an optimal balance between smoothness and consistency. This trend validates the effectiveness of the proposed multi-objective loss formulation in guiding noise level selection. The optimal q values identified for EKF, AKKF, and MHE are approximately 5.3367×10^{-8}, 1.4175×10^{-9}, and 7.5646×10^{-9} respectively. Furthermore, the parameters used in this paper are summarized in Table 3.

4.3.2. RUL estimation results and analysis

In this section, different estimators are used for RUL estimation based on the $BPOO_{EESCor}$.

The performance of RUL estimation is illustrated in Figure 12, which presents both the estimated HI trajectories and the corresponding RUL prediction results obtained using three estimators: EKF, AKKF, and MHE. To quantitatively assess the accuracy of these estimators, several evaluation metrics are introduced below. The effectiveness of a prognostic model can be assessed using various evaluation criteria, as discussed in (Saxena, Goebel, Simon, & Eklund, 2010; Liu, Pluymers, Desmet, & Gryllias, 2022). Among

Table 3. Parameter list.

Parameters	Value
Failure threshold	0.1
Training set	30
λ_1	0.7
λ_2	0.3
Search range of q	$[10^{-10}, 10^{-4}]$
Measurement Noise R_n	3.9713×10^{-6}
Process Noise Level q_n	5.3367×10^{-8} (EKF) 1.4175×10^{-9} (AKKF) 7.5646×10^{-9} (MHE)

Table 4. Performance comparison of different estimators.

Metric	EKF	AKKF	MHE
RMSE (x 6 mins)	3598.5	234.19	2927.5
MAE (x 6 mins)	659.25	108.25	399.39
CRA	-1.9231	-0.048602	-1.1902

them, two widely used error-based indicators are the Root Mean Squared Error (RMSE) and the Mean Absolute Error (MAE), which quantify the discrepancy between the actual Remaining Useful Life (RUL_{act}) and the predicted Remaining Useful Life (RUL_{pred}). Given a total of N samples, these two metrics are defined as follows:

$$\text{RMSE} = \sqrt{\frac{1}{N} \sum_{i=1}^{N} \left(RUL_{act}^i - RUL_{pred}^i \right)^2} \qquad (15)$$

$$\text{MAE} = \frac{1}{N} \sum_{i=1}^{N} \left| RUL_{act}^i - RUL_{pred}^i \right| \qquad (16)$$

Besides, from a practical standpoint, achieving higher prediction precision near the end of life is often more critical for decision-making than at earlier degradation stages. To emphasize this, the Cumulative Relative Accuracy (CRA) metric has been proposed, which assigns increasing importance to later time steps. CRA is calculated as:

$$CRA = \sum_{i=1}^{N} \omega_i RA_i \qquad (17)$$

Here, RA_i denotes the relative accuracy at the i-th time step, while ω_i is the corresponding weighting factor. These quantities are defined by:

$$RA_i = 1 - \frac{\left| RUL_{act}^i - RUL_{pred}^i \right|}{RUL_{act}} \qquad (18)$$

$$\omega_i = \frac{i}{\sum_{i=1}^{N} i} \qquad (19)$$

A higher value of CRA (closer to 1) suggests better prognostic capability. The matrices for the estimation results of three estimators are listed in Table 4. It shows that the AKKF estimator obtains the best performance among these three estimators.

In Figure 12 (a), all three methods successfully track the observed HI trajectory while maintaining relatively smooth trends. This consistency in HI estimation is crucial, as the RUL predictions shown in Figure 12 (b) are directly derived from these estimated HI values. The RUL estimates exhibit varying degrees of stability and accuracy across the different methods.

The EKF results show significant fluctuations, with frequent overestimation and underestimation of the RUL. These erratic behaviors suggest that EKF is more susceptible to noise and abrupt changes in the HI.

In contrast, the AKKF yields the most stable and accurate RUL predictions, closely following the ideal linear degradation trend with a slope of -1. This demonstrates the advantage of adaptive kernel-based method in handling nonlinear degradation patterns and suppressing stochastic disturbances.

The MHE also produces smooth RUL estimates comparable to those from the AKKF, but it occasionally shows a delayed response to changes in the HI. This lag is likely due to the inherent nature of the moving window used in MHE, which may introduce slight latency in prediction updates.

Importantly, all three methods generally preserve the expected inverse relationship between the HI and RUL: lower HI values correspond to higher remaining life. However, the HI is not strictly monotonic — fluctuations may occur due to physical effects such as surface polishing or changes in ball-to-race contact conditions as the fault develops. Despite these irregularities, both AKKF and MHE maintain reliable long-term degradation tracking, highlighting their robustness and suitability for real-world applications where such HI variations are common. These observations suggest that both the construction and selection of HIs, as well as the incorporation of physical constraints on RUL, remain critical areas for future investigation to further improve prognostic accuracy.

5. CONCLUSION

This paper presents a Kalman-based framework for RUL prognostics of rolling element bearings under time-varying operating conditions. By extracting order-domain features that capture cyclostationary behavior, the framework effectively handled non-stationary vibration signals caused by variable speed. A probabilistic fault detection strategy based on multiple HIs improved fault onset identification and reduced false alarms, as experimental results showed that re-
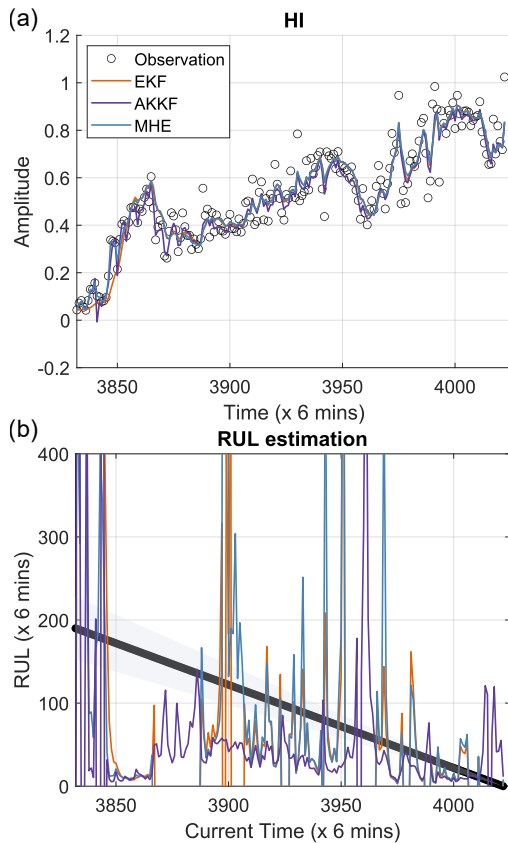
Figure 12. HI estimation and the estimated RULs: (a) HI estimation; (b) RUL estimation

lying on a single HI can lead to early or missed detections. Furthermore, a data-driven approach, to optimize the process and the measurement noise covariances, enhanced the stability and the prediction accuracy of the Kalman-based estimators. The final RUL estimation results indicate that the AKKF-based estimator achieves the best results.

While the current framework successfully addresses speed variation and multi-indicator fusion, several opportunities remain for further improvement. First, explicit segmentation and modeling of load variations should be considered to better capture their influence on degradation. Second, incorporating additional data sources—such as temperature, torque, or strain—may enhance the robustness and informativeness of the prognostic model. Finally, future work will explore extending the proposed noise covariance optimization strategy to online or adaptive settings, enabling real-time tuning of the Kalman filter under dynamically changing operating conditions.

REFERENCES

Antoni, J., Xin, G., & Hamzaoui, N. (2017). Fast computation of the spectral correlation. *Mechanical Systems and Signal Processing*, *92*, 248-277. doi: https://doi.org/10.1016/j.ymssp.2017.01.011

Cui, L., Wang, X., Xu, Y., Jiang, H., & Zhou, J. (2019). A novel switching unscented kalman filter method for remaining useful life prediction of rolling bearing. *Measurement*, *135*, 678-684. doi: https://doi.org/10.1016/j.measurement.2018.12.028

Gabrielli, A., Battarra, M., Mucchi, E., & Dalpiaz, G. (2024). Physics-based prognostics of rolling-element bearings: The equivalent damaged volume algorithm. *Mechanical Systems and Signal Processing*, *215*, 111435. doi: https://doi.org/10.1016/j.ymssp.2024.111435

Li, Y., Huang, X., Ding, P., & Zhao, C. (2021). Wiener-based remaining useful life prediction of rolling bearings using improved kalman filtering and adaptive modification. *Measurement*, *182*, 109706. doi: https://doi.org/10.1016/j.measurement.2021.109706

Li, Z., Zhu, R., Verwimp, T., Wen, H., & Gryllias, K. (2025). Estimation of remaining useful life of rolling element bearings based on the adaptive kernel kalman filter. *Mechanical Systems and Signal Processing*, *229*, 112493. doi: https://doi.org/10.1016/j.ymssp.2025.112493

Lim, C. K. R., & Mba, D. (2015). Switching kalman filter for failure prognostic. *Mechanical Systems and Signal Processing*, *52-53*, 426-435. doi: https://doi.org/10.1016/j.ymssp.2014.08.006

Liu, C., Pluymers, B., Desmet, W., & Gryllias, K. (2022). A digital twin-assisted deep learning model for rolling element bearing prognostics. In *Proceedings of 2022 international conference on noise and vibration engineering (isma 2022)*.

Ma, X., Yan, B., Wang, H., & Liao, H. (2023). A hybrid prognostic method for rotating machinery under time-varying operating conditions by fusing direct and indirect degradation characteristics. *Measurement*, *214*, 112831. doi: https://doi.org/10.1016/j.measurement.2023.112831

Mauricio, A., & Gryllias, K. (2021). Cyclostationary-based multiband envelope spectra extraction for bearing diagnostics: The combined improved envelope spectrum. *Mechanical Systems and Signal Processing*, *149*, 107150. doi: https://doi.org/10.1016/j.ymssp.2020.107150

Mauricio, A., Smith, W. A., Randall, R. B., Antoni, J., & Gryllias, K. (2020). Improved envelope spectrum via feature optimisation-gram (iesfogram): A

novel tool for rolling element bearing diagnostics under non-stationary operating conditions. *Mechanical Systems and Signal Processing*, *144*, 106891. doi: https://doi.org/10.1016/j.ymssp.2020.106891

Qi, J., Zhu, R., Liu, C., Mauricio, A., & Gryllias, K. (2024). Anomaly detection and multi-step estimation based remaining useful life prediction for rolling element bearings. *Mechanical Systems and Signal Processing*, *206*, 110910. doi: https://doi.org/10.1016/j.ymssp.2023.110910

Saxena, A., Goebel, K., Simon, D., & Eklund, N. (2010). Damage propagation modeling for aircraft engine run-to-failure simulation. *International Journal of Prognostics and Health Management*, *1*(1), 1–17.

Singleton, R. K., Strangas, E. G., & Aviyente, S. (2015). Extended kalman filtering for remaining-useful-life estimation of bearings. *IEEE Transactions on Industrial Electronics*, *62*(3), 1781-1790. doi: 10.1109/TIE.2014.2336616

SKF Evolution Team. (2024). *Condition monitoring with ai at your elbow.* (Accessed: 2025-07-07)

Soave, E., D'Elia, G., & Dalpiaz, G. (2023). Prognostics of rotating machines through generalized gaussian hidden markov models. *Mechanical Systems and Signal Processing*, *185*, 109767. doi: https://doi.org/10.1016/j.ymssp.2022.109767

Vencl, A., Gašić, V., & Stojanović, B. (2017, feb). Fault tree analysis of most common rolling bearing tribological failures. *IOP Conference Series: Materials Science and Engineering*, *174*(1), 012048. doi: 10.1088/1757-899X/174/1/012048

Wang, D., Zhao, X., Kou, L.-L., Qin, Y., Zhao, Y., & Tsui, K.-L. (2019). A simple and fast guideline for generating enhanced/squared envelope spectra from spectral coherence for bearing fault diagnosis. *Mechanical Systems and Signal Processing*, *122*, 754-768. doi: https://doi.org/10.1016/j.ymssp.2018.12.055

Wen, Y., Fashiar Rahman, M., Xu, H., & Tseng, T.-L. B. (2022). Recent advances and trends of predictive maintenance from data-driven machine prognostics perspective. *Measurement*, *187*, 110276. doi: https://doi.org/10.1016/j.measurement.2021.110276

Zhang, L., Sidoti, D., Bienkowski, A., Pattipati, K. R., Bar-Shalom, Y., & Kleinman, D. L. (2020). On the identification of noise covariances and adaptive kalman filtering: A new look at a 50 year-old problem. *IEEE Access*, *8*, 59362-59388. doi: 10.1109/ACCESS.2020.2982407

BIOGRAPHIES

Zhen Li joined the Noise and Vibration Research Group in the Department of Mechanical Engineering at KU Leuven, Belgium, as a PhD researcher in 2022. His research interests lie in the areas of remaining useful life prognostics of rotating machine using state estimation technologies.

Panagiotis Mantas received his Bachelor and Master of Engineering degree in Mechanical Engineering from University of Patras, Greece. He joined the Noise and Vibration Research Group in the Department of Mechanical Engineering at KU Leuven, Belgium, as a PhD researcher in 2023. His research interests lie in the areas of rotating machine bearing measurements and diagnostics using Optical Fiber Bragg Grating sensors.

Toby Verwimp received his MSc in mechanical engineering from KU Leuven, Leuven, Belgium in 2021. He joined the LMSD (Mecha(tro)nic System Dynamics) Division in the Department of Mechanical Engineering at KU Leuven as a PhD researcher in 2021. His research interests include condition monitoring of rotating machinery using, among others, rotary encoders and cameras.

Alexandre Mauricio received his MSc. degree in Mechanical Engineering from the Faculty of Engineering of the University of Porto (FEUP) in 2017. Then he obtained his Ph.D. degree at the Department of Mechanical Engineering of KU Leuven, Belgium. His main research interests focus on the diagnostics of rotating machinery operating under time varying conditions.

Konstantinos Gryllias received his Diploma and Ph.D. degrees in Mechanical Engineering from the National Technical University of Athens, Athens, Greece, in 2004 and 2010, respectively. He is currently Professor of Vibro-acoustics of machines and transportation systems at the Department of Mechanical Engineering, KU Leuven, Leuven, Belgium. He also serves as the Manager of the University Core Lab Flanders Make@KU Leuven Motion Products, Belgium. His research interests include condition monitoring, signal processing, prognostics, and health management of mechanical and mechatronic systems.